Chemical characterisation of bitumen type and ageing state based on FTIR spectroscopy and discriminant analysis integrated with variable selection methods

Ma, Lili; Varveri, Aikaterini; Jing, Ruxin; Erkens, Sandra

DOI
10.1080/14680629.2023.2181008

Publication date
2023

Document Version
Final published version

Published in
Road Materials and Pavement Design

Citation (APA)
Ma, L., Varveri, A., Jing, R., & Erkens, S. (2023). Chemical characterisation of bitumen type and ageing state based on FTIR spectroscopy and discriminant analysis integrated with variable selection methods. *Road Materials and Pavement Design*, *24*(S1), 506-520. https://doi.org/10.1080/14680629.2023.2181008

Road Materials and Pavement Design

ISSN: (Print) (Online) Journal homepage: https://www.tandfonline.com/loi/trmp20

Chemical characterisation of bitumen type and ageing state based on FTIR spectroscopy and discriminant analysis integrated with variable selection methods

Lili Ma, Aikaterini Varveri, Ruxin Jing & Sandra Erkens

To cite this article: Lili Ma, Aikaterini Varveri, Ruxin Jing & Sandra Erkens (2023): Chemical characterisation of bitumen type and ageing state based on FTIR spectroscopy and discriminant analysis integrated with variable selection methods, Road Materials and Pavement Design, DOI: 10.1080/14680629.2023.2181008

To link to this article: https://doi.org/10.1080/14680629.2023.2181008

Published online: 01 Mar 2023.

ROAD MATERIALS AND PAVEMENT DESIGN
https://doi.org/10.1080/14680629.2023.2181008

Taylor & Francis
Taylor & Francis Group

Chemical characterisation of bitumen type and ageing state based on FTIR spectroscopy and discriminant analysis integrated with variable selection methods

Lili Ma, Aikaterini Varveri, Ruxin Jing and Sandra Erkens

Faculty of Civil Engineering and Geosciences, Delft University of Technology, Delft, Netherlands

ABSTRACT

The chemical characterization of bitumen type and ageing state are fundamental in determining structural and mechanical properties of bitumen. This work aims to classify various bitumen types at different ageing states and to identify the primary chemical differences relevant to the classification. Fourier transform infrared (FTIR) spectral data of eight bitumen types at five ageing states were analyzed using a chemometric procedure that incorporates principal component analysis (PCA), linear discriminant analysis (LDA) models, variable selection methods. The models presented results of high accuracy in differentiating bitumen type and ageing state. The results show that the spectral regions that describe the aliphatic and aromatic bonds are critical to the identification of bitumen types. The chemical changes due to bitumen ageing are mainly revealed at the region of 1800 – 900 cm-1. This chemometric method is instructive for the characterization of chemical bitumen properties.

ARTICLE HISTORY
Received 12 October 2022
Accepted 9 February 2023

KEYWORDS
Bitumen; FTIR; source; ageing; multivariate analysis; variable selection

1. Introduction

Bitumen is a byproduct of crude oil distillation, composed of complex hydrocarbons which can be classified into saturates, aromatics, resins and asphaltenes, typically known as SARA fractions (Sakib & Bhasin, 2019). The chemical composition of bitumen governs the structural and mechanical properties, such as strength, stiffness, and colloidal structure (Dehouche et al., 2012; Sakib et al., 2020). Bituminous binders with various crude oil sources, penetration grades, polymer modifiers, and additives are used for paving asphalt pavements. Understanding the complex chemical components in bitumen is therefore important for characterising the mechanical properties of bitumen and paving mixtures.

Chemical composition of bitumen depends on its crude source and varies with its ageing state (Mirwald et al., 2020a; Petersen, 2000). Bitumen from different crude oil sources, even with the same specifications such as penetration grade, can have widely different SARA fractions and exhibit diverse ageing kinetics. Mechanisms of bitumen ageing include oxidation, evaporation of light components, and physical (steric) hardening (Tauste et al., 2018), among which oxidation is reported as the primary factor. Bitumen oxidation is an oxygen diffusion-driven process, which can be accelerated by UV radiation (Polo-Mendoza et al., 2022). The chemical procedure of bitumen oxidation normally consists of the dehydrogenation, the production of new functional groups, and the increase in aromaticity

CONTACT Lili Ma lili.m@tudelft.nl

(aromatic condensation) (Nivitha et al., 2016; Polo-Mendoza et al., 2022; Tauste et al., 2018). Ageing causes a significant reduction of the aromatic fraction and growth in the content of resins and asphaltenes, which results in an increase in the polarity, acidity, viscosity, and stiffness of bitumen (Mirwald et al., 2020b). This ultimately leads to bitumen embrittlement (Lukas et al., 2015), and can cause ravelling and cracking of pavements (López-Montero & Miró, 2016).

Fourier transform infrared (FTIR) spectroscopy is a quick and powerful technique in characterising the chemical composition of bitumen and its SARA fractions (Mirwald et al., 2020a; Pipintakos et al., 2021). To evaluate the chemical changes in bitumen samples at different ageing states, characteristic peaks and regions of FTIR spectra such as sulfoxides, carbonyls, aliphaticity, and aromaticity are usually determined (Hofko et al., 2017). Among them, the sulfoxide (1030 cm^{-1}) and carbonyl (1700 cm^{-1}) peaks have been successfully used to describe the degree of ageing and are linked to the physical and rheological properties of bitumen (Herrington, 2012; Pipintakos et al., 2022). Other functional groups with lower intensities in FTIR spectra are attracting more and more attention. For example, a change from 2-quinoloes (1655 cm^{-1}) and carboxylic acids (1730 cm^{-1}) towards ketones (1700 cm^{-1}) is reported (Mirwald et al., 2020a), which describes the chemical process of the formation of ketones. The overlap of spectral regions indicating different functional groups (Asemani & Rabbani, 2020) and the shift of the fingerprint area caused by increased polarity (Mirwald et al., 2020a) make it rather difficult to monitor the change of functional groups during the ageing process. Moreover, the change in aliphaticity and aromaticity with bitumen source and ageing state is also inconclusive (Feng et al., 2015). The evolution of aromatic bands (1600 cm^{-1}) with ageing is not evident and thus less used as an ageing index even though the increase in aromaticity is well-known (Pipintakos et al., 2021; Redelius & Soenen, 2015).

For bitumen samples with varying sources or ageing states, the chemical differences are shown in the whole absorption spectra, and the consideration of specific peaks may not be sufficient in distinguishing their complex chemical composition. Alternatively, chemometric approaches using multivariate discriminant methods, such as principal component analysis (PCA), Hierarchical cluster analysis (HCA), linear discriminant analysis (LDA), and partial least squares (PLS) analysis (Khanmohammadi et al., 2012), have been receiving increasing attention in extracting useful chemical information from the FTIR spectra. Recent studies have used FTIR spectra integrated with chemometrics to precisely identify bitumen sources (Weigel & Stephan, 2018), determine bitumen SARA fractions (Meléndez et al., 2012; Mohammadi et al., 2021; Ren et al., 2019), and predict the physical and mechanical properties of bitumen (Siroma et al., 2021; Sun et al., 2020). Wilt and Welch (1998) predicted the asphaltene content in crude oil using a PLS model with an R^2 value of 0.95. Aske et al. (2001) reported a high accuracy of PCA and PLS in determining bitumen SARA fractions based on FTIR spectra. Weigel and Stephan (2018) differentiated bitumen types and ageing states using PCA and LDA models and predicted the rheological properties based on PLS analysis.

Despite the good predictions of multivariate methods based on multiple variables, the latent variables derived from the features of full FTIR spectra are less interpretable compared to original variables (Xiaobo et al., 2010). Furthermore, among the large number of spectral variables, irrelevant and noisy variables may yield harmful variations in the prediction results. To this end, variable selection has been used to identify and select a small number of variables from original variable sets for good interpretation and prediction. Widely-used variable selection methods include the genetic algorithm (GA), simulated annealing (SA), moving windows (MW), and competitive adaptive reweighted sampling (CARS) methods. Li et al. (2019) discussed different variable selection methods from the perspective of identifying the penetration grade of bitumen. It was found that the CARS coupling with Support Vector Machine (SVM) showed the best performance. Mohammadi et al. (2021) applied a hybrid of GA and SVM regression (GA-SVM-R) model to predict the SARA fractions of bitumen. Compared to GA-PLS-R, the GA-SVM-R model exhibits better performance in the quantitative determination of the SARA fractions. The variable selection methods can support an advanced analysis, however, to the best of our knowledge, these methods have not yet been applied to study the chemical differences of various bitumen types at different ageing states.

This paper aims to investigate the chemical information from FTIR data that is relevant to the identification and classification of bitumen types and ageing states. To this end, MW and SA variable selection methods were used to identify important wavelength regions with respect to bitumen type and ageing state, and then multivariate PCA, LDA, and PCA-LDA models were applied and compared with regard to their prediction accuracy.

2. Materials and methods

2.1. Materials

To study the chemical properties of bitumen from various crude oil sources, and with various penetration grades, polymer modifiers (Styrene–butadiene–styrene (SBS)), and ageing states, 40 binder samples of eight binder types at four ageing states were prepared, as described below:

- Bitumen obtained from source Q, with penetration grades 40/60, 70/100, and SBS modifier (with 70/100 as base bitumen), denoted as Q460, Q710, and QPMB, respectively;
- Bitumen obtained from source T, with penetration grades 70/100, 100/150, and 160/220, denoted as T710, T1015, and T1622, respectively;
- Bitumen obtained from source V, with penetration grades 70/100 and SBS modifier (with 70/100 as base bitumen), denoted as V710 and VPMB, respectively.

For each bitumen type, a can of fresh binder was heated up to 140°C for 5 min and poured into four containers with a diameter of 140 mm. Each container weighed 50.0 ± 0.5 g. These containers were then placed in oven at 140°C for 5 min to obtain a thin bitumen film of 3.2 mm. Four containers were aged at four states comprising one short-term ageing protocol and one long-term ageing protocol with three different ageing times. Short-term ageing was simulated by the thin film oven test (TFOT) at 163°C for five hours, which is referred to as Oven. Long-term aged samples were prepared using a combination of the TFOT protocol followed by ageing in the Pressure Ageing Vessel (PAV) at 2.1 MPa and 100°C for 20 h (1P), 40 h (2P), and 80 h (4P).

2.2. Test methods

FTIR spectroscopy was carried out using the Attenuated Total Reflection (ATR) mode. For each sample, three independent measurements were performed. A wavelength range of 4000–600 cm^{-1} with a resolution of 1 cm^{-1} and 32 scans were applied. The spectral regions of 2400–1900 cm^{-1} and 4000–3700 cm^{-1} were manually removed and were not considered for further discriminant analysis because of the poor quality of the chemical information in these ranges (Weigel & Stephan, 2017).

The chemical information of the FTIR spectra is shown in Figure 1. The mid-infrared FTIR spectral region of 4000–600 cm^{-1} is informative of the aliphaticity, aromaticity, heteroatom-based functionality, and oxygenation of bitumen components. Most of the absorption peaks are assigned to different types of C–H vibrations. The band between 3050 and 3000 cm^{-1} is assigned to the C–H stretching of cis double bonds and aromatics. The bands ranging from 2965 to 2946 cm^{-1} and from 2876 to 2864 cm^{-1} are representative of the antisymmetric and symmetric C–H stretching vibrations of CH_3 groups, respectively. For CH_2 groups, the antisymmetric and symmetric vibration bands are 2946–2880 cm^{-1} and 2864–2825 cm^{-1}. The aliphatic $-CH_2$ and $-CH_3$ bending vibrations are shown at band areas of 1485–1400 cm^{-1} and 1400–1357 cm^{-1}. Specifically, the peak at 722 cm^{-1} indicates the presence of long alkyl chain groups in saturates, i.e. $(CH_2)_n$, where n is larger than 4. The C–H bending vibration of aromatic groups is at 3100–3000 cm^{-1}, and the bands between at 900–838 cm^{-1}, 838–783 cm^{-1}, and 783–732 cm^{-1} are attributed to various aromatic C–H in-plane and out-of-plane bending vibrations. The multiple C = C stretching vibrations are at 1600 cm^{-1} (Castro & Vazquez, 2009).

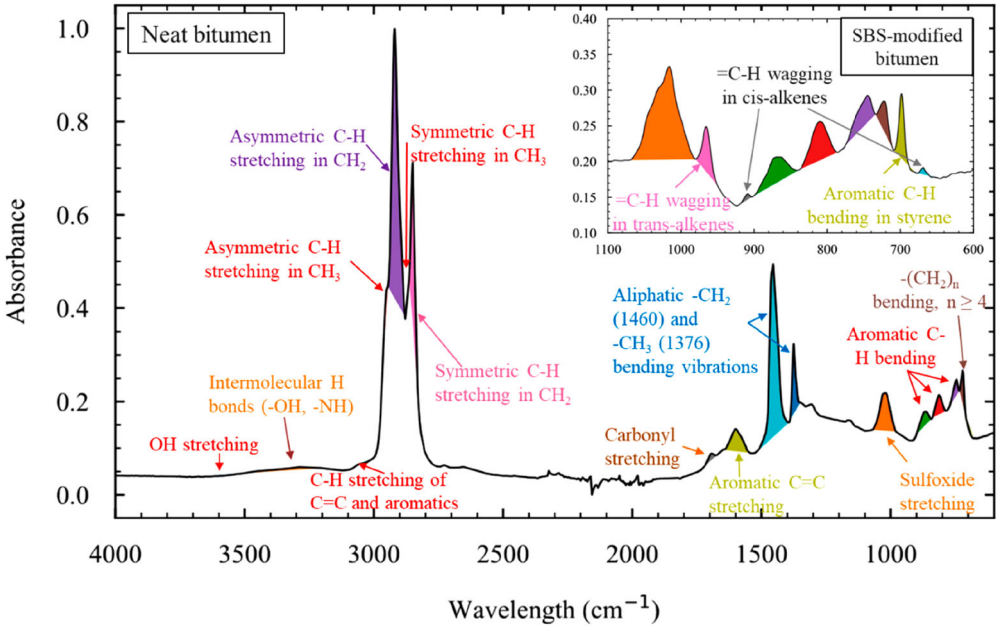

Figure 1. FTIR spectra of neat bitumen (4000–600 cm^{-1}) and SBS-modified bitumen (1100–600 cm^{-1}).

The peaks describing heteroatom-based functional groups are observable in FTIR spectra. The absorption bands at 3650–3500 cm^{-1} denote the OH stretching. The bands of 3500–3200 cm^{-1} show the intermolecular hydrogen bonds (–OH, –NH) in phenolic, alcoholic, and carboxylic acids. The regions between 1750 and 1610 cm^{-1} are attributed to the stretching vibrations of carbonyl functional groups (including esters, ketones, aldehydes, and carboxylic acids) (Asemani & Rabbani, 2020), and the peaks at 1310, 1260, 1160, 1080, 1030, and 810 cm^{-1} are sulfur-containing functional groups, i.e. sulfoxides, sulfones and sulfate ester (Mirwald et al., 2020a). Both the carbonyl- and sulfur-based functional groups are crucial for the chemical changes of binders due to ageing (Buenrostro-Gonzalez et al., 2002; Petersen, 2009). Nitrogen-based functional groups are found at ca. 3239 cm^{-1} (N–H stretching in amides), 1575 cm^{-1} (N-H bending in amides), and 1310 cm^{-1} (C–N bending in pyridine, pyrrole, and amides) (Asemani & Rabbani, 2020; Gabrienko et al., 2015). The peaks and regions denoting these functional groups can overlap with other chemicals and have low intensity in FTIR spectra (Asemani & Rabbani, 2020; Zojaji et al., 2021). Therefore, they are less discussed in literature than the carbon and sulfur related ones.

The SBS modifier consists of a polybutadiene (PB) segment in the middle with polystyrene (PS) blocks at the end. The representative FTIR peaks of SBS-modified bitumen are the out-of-plane wagging of $=$C–H in cis- and trans-alkenes at 670, 910, and 966 cm^{-1}, the aromatic C–H bending in styrene at 699 cm^{-1}, the aliphatic –[CH_2]– at 1450 cm^{-1}, and C–C aromatic rings at ca. 1490 cm^{-1}. The last two peaks overlap with the peaks of neat bitumen spectra (Kumar et al., 2020). During the ageing process, polystyrene remains stable while polybutadiene shows a reduction in peak intensities that denotes polymer degradation due to chain scission.

2.3. Variable selection methods

In this work, two variables selection methods were used to optimise the discriminant analysis, i.e. the MW and the SA methods. The MW selection method allows the selection of a narrower wavelength region than the full spectral region, which is more representative for the differentiation of observations. To achieve this, two variables are to be optimised, i.e. the window size and the window range. In

the present work, considering that the area of most peaks (Figure 1) is wider than 50 cm^{-1}, the window sizes in the range of 50–800 cm^{-1} (ca. a quarter of whole spectra) with a step of 50 cm^{-1} were analysed. For each window size, a series of band intervals were generated by moving the window through the whole spectra with a moving step of 25 cm^{-1}. The determination of optimal window size and window range was based on the prediction accuracy (the fraction of correctly classified samples).

On the other hand, the SA method is a probabilistic global optimisation technique that is primarily used to find the global optimum in the presence of large numbers of local optima (Kirkpatrick et al., 1983). This method simulates the annealing of crystals after heating to a temperature to reach its minimum internal energy in thermodynamics, which depends on the initial temperature and rate of cooling. Compared to the annealing in materials, simulated annealing uses the objective function of an optimisation problem instead of the energy of a material. This method starts with a random selection of a subset of all variables (all wavelengths in a measured FTIR spectra), and then the prediction accuracy is calculated. Part of the variables in the subset are then exchanged with variables outside of the subset, and the prediction accuracy is evaluated for a second time. The new variable set is accepted if the new prediction accuracy is higher than the previous one. When the new set has lower accuracy, there is still a probability (*po*) to accept the exchange process that is quantified by

$$po(\Delta S) = \exp\left(\frac{-\Delta S}{T}\right) \tag{1}$$

where ΔS is the difference between the current and previous prediction accuracies, and T is a predefined cooling factor, which is determined so as to obtain a fair probability; not too large to hinder convergence or too small to allow for occasional fluctuation. The acceptance of non-improving steps is to avoid being frozen at a local optimum. The maximum iteration time is also needed to designate the end of the selection procedure. For the SA method in this work, the number of variables ranging from 10 to 180 with a step of 10 were compared. The maximum iteration time was defined as 150. Trial discriminant modelling results with regard to bitumen type and ageing state showed that the prediction accuracy had limited improvement after 150 iterations.

2.4. Multivariate discriminant models

Prior to discriminant analysis, the FTIR spectra data was preprocessed to eliminate unwanted variations arising from instrumental drifts and differences in sample preparation (Hofko et al., 2017). The standard normal variate (SNV) was used to correct wavenumber scaling and background effects. The Savitzky–Golay (SG) was performed for smoothing the mid-infrared spectra and obtaining the first derivative of the spectra to reduce the overlap of peaks, accentuate small structural differences between similar spectra, and to avoid issues with baseline shifting (Meléndez et al., 2012).

After preprocessing of spectral dataset, the FTIR data (3700–2400 cm^{-1} and 1900–900 cm^{-1}) with a resolution of 1 cm^{-1} were merged into a resolution of 5 cm^{-1}. Therefore 560 spectra variables were ultimately considered for multivariate analysis using chemometric methods.

Chemometric methods, such as PCA, PLS, and LDA, are used for sample classification and pattern recognition, by determining mathematical relationships between a set of descriptive variables (e.g. chemical spectral information) and qualitative variables (e.g. defined class). PCA is primarily used to transform datasets with many variables into uncorrelated components to reduce dimensionality. The scores of target samples are calculated as

$$\mathbf{Y} = \mathbf{X} \times \mathbf{W} \tag{2}$$

where $\mathbf{X}$ is the dataset composed of m samples (divided into l groups) and n variables, $\mathbf{W}$ is a $n \times p$ loading matrix where p is the number of selected principal components, and $\mathbf{Y}$ is a $m \times p$ score matrix describing the projection of $\mathbf{X}$ into a p-dimensional feature subspace. To obtain $\mathbf{W}$, the eigenvectors

and eigenvalues of the covariance matrix of the variables in a spectra dataset are calculated. The eigenvalues are then sorted in descending order and p eigenvectors with largest eigenvalues are selected to construct **W**.

LDA is a linear discriminant analysis method which performs supervised dimensionality reduction by selecting the space directions that achieve a maximum separation among the different classes according to the Euclidean distance. Therefore, the loading matrix **W** of LDA minimises the scatter within each class and maximises the scatter among classes. LDA can only project datasets to a dimensional space lower than the number of classes l.

In the PCA-LDA modelling approach, first the PCA model is performed to reduce the number of variables and retain as much variance as possible. The PCA-extracted variables are then used to perform LDA modelling. In the PCA-LDA model, the loading matrix **W** is the dot product of the loading matrix of PCA ($n \times p$) and LDA ($p \times q$), and thus has a size of $n \times q$ where q is the selected number of components in LDA.

To analyse the FTIR datasets and differentiate among bitumen types and ageing states, PCA, LDA, and PCA-LDA models were utilised. Spectra of all bitumen samples (40 binders and with three replicates per sample) were collected for the differentiation of both bitumen type and ageing state. These spectra were preprocessed to eliminate unwanted information, and then subsets of variables were obtained from the spectra by means of the MW and SA variable selection methods. The prediction accuracies of PCA, LDA, and PCA-LDA modelling utilising the selected variables were evaluated. To quantify the robustness of these models (PCA, LDA and PCA-LDA) and avoid overfitting, a 5-fold cross-validation method was applied. This method divides the whole dataset into 5 sub-sets, uses four of them as training datasets, and discriminant results are validated on the remaining data (testing data) to obtain the prediction accuracy. Five different combinations of training and testing data can be generated, and the ultimate prediction accuracy of the model is the average of the five loops. The prediction accuracy of the three models was compared and the variable sets with the best prediction performance were used for the discriminant analysis of bitumen types and ageing states.

3. Results and discussion

3.1. FTIR results

Figure 2 shows the mid-infrared original spectra and their first derivatives for all bitumen samples from different sources at various ageing states. Compared to the original spectra, the differences in the first derivatives caused by baseline shifting are removed, as demonstrated by the standard deviation of original spectra and first derivatives in Figure 2. Large deviations are shown in the band areas of ca. 3000–2800 cm^{-1} and 1700–700 cm^{-1}. The chemical information of these wavelengths are described in Figure 1.

Figure 3 depicts the FTIR spectra of all bitumen types at fresh conditions. In Figure 3(a), the differences between the neat (pure) and modified bitumen are shown at wavenumbers of ca. 965, 910, and 695 cm^{-1}. The V710 and VPMB samples show similar spectra since VPMB uses V710 as base bitumen; this also holds for the Q460 and Q710 samples and the T710, T1015, and T1622 samples that are produced from the same crude oil source. The sulfoxide peak of T1622 at 1030 cm^{-1} is smaller than that of T1015 and T710, and the peak intensities between 1800 and 1640 cm^{-1} are also lower for T1622. This indicates that T1622 has less functional groups. Figure 3(b) depicts the spectral regions of 3100–2700 cm^{-1} for all bitumen types. All bitumen types show similar peak positions and intensities. Therefore, advanced methods are needed to differentiate bitumen types based on this range.

The spectra of Q710, T710, and VPMB samples at all ageing states are shown in Figure 4. The peaks of carbonyl and sulfoxide increase with ageing states for all three bitumen types, while the change in 965 and 695 cm^{-1} with increasing ageing levels is not obvious.

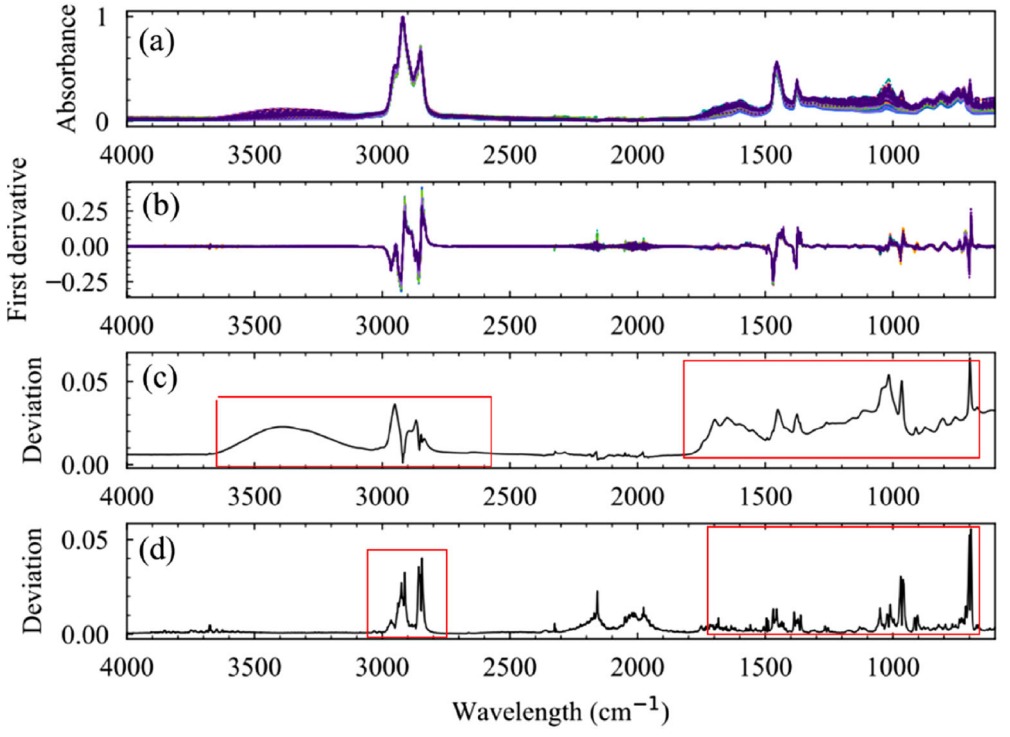

Figure 2. (a) Original FTIR spectra and (b) first derivative of FTIR spectra of bitumen; (c) standard deviation of original spectra, and (d) standard deviation of first derivatives of all bitumen spectra.

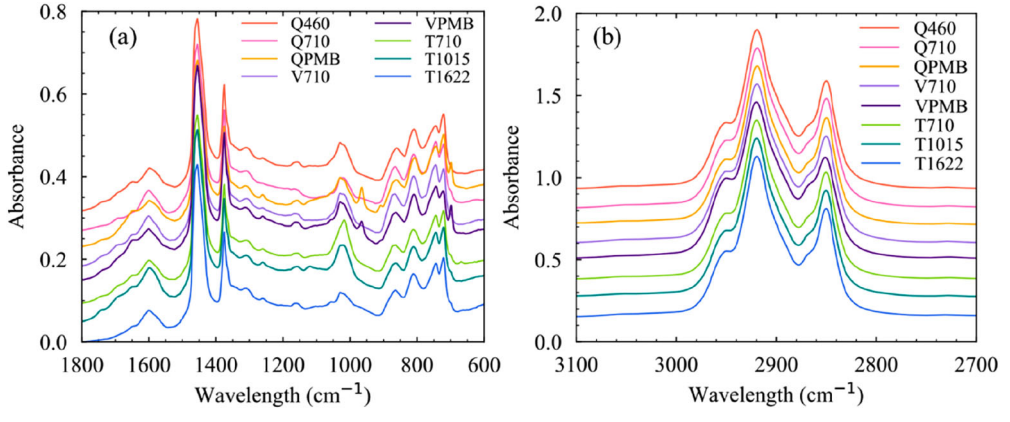

Figure 3. FTIR spectra (average of three replicates for each sample) of fresh bitumen from different sources at wavenumbers of (a) 1800–600 cm^{-1} and (b) 3100–2700 cm^{-1}.

3.2. Evaluation of discriminant models and variable selection methods

Figure 5 shows the PCA score plots marked based on bitumen type and ageing state. It can be seen that PCA fails to distinguish bitumen samples with different types or at different ageing states. Therefore, the supervised classification method, i.e. LDA was used which uses both spectra data and classifications of samples as input data.

To compare the multivariate analysis results of the peaks and the full spectra using LDA and PCA-LDA models, the areas of all the peaks described in Figure 1 were calculated using the tangential

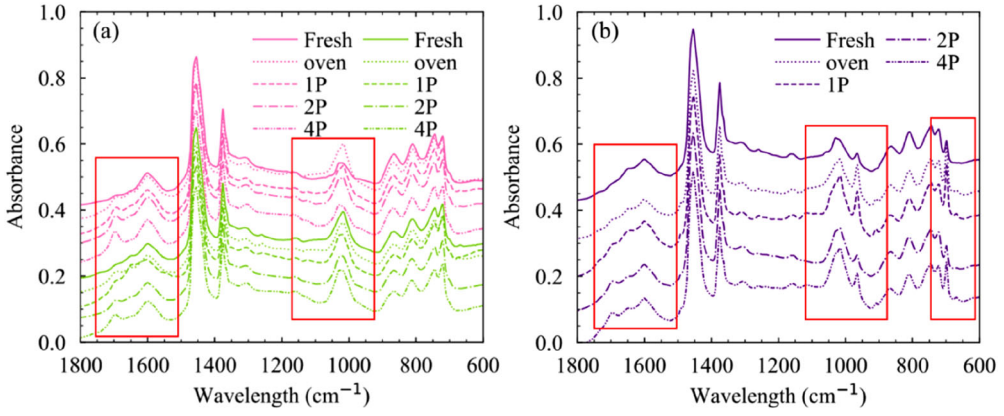

Figure 4. FTIR spectra (averages of three replicates for each sample) of bitumen at different ageing states: (a) Q710 (upper five spectra) and T710 (lower five spectra), and (b) VPMB samples.

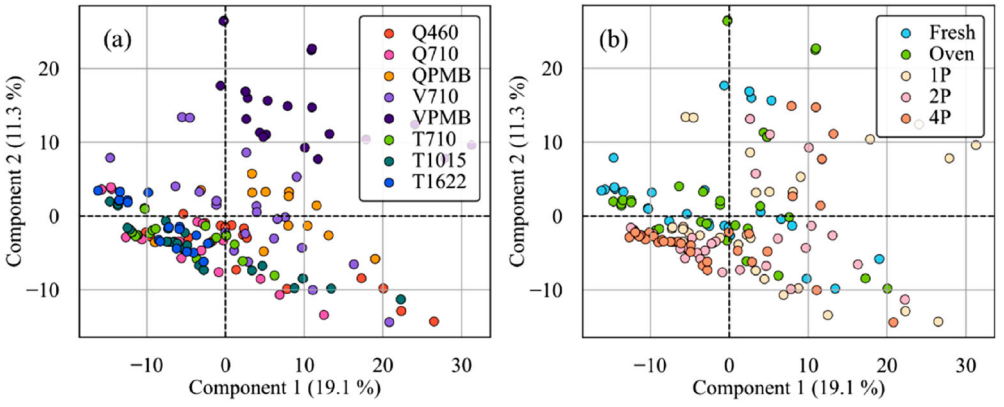

Figure 5. PCA score plots based on (a) bitumen types and (b) ageing states.

integration method (Hofko et al., 2017). The prediction accuracies of LDA and PCA-LDA based on the peaks and the full spectra are listed in Table 1. The accuracy of predicting the crude oil source is 1.0 for all the combinations of analysis (namely considering peaks and full spectral data) except for the LDA modelling using spectral data. The prediction accuracy of the ageing state is lower than the accuracy of bitumen source and type. This is due to the higher similarities of the FTIR spectra of bitumen at different ageing states compared to bitumen source and type. The performance of LDA and PCA-LDA is similar for all the analysis cases. Classification models considering only the peak data seem to exhibit slightly higher prediction accuracy. The LDA and PCA-LDA models using full spectra may take noisy information into consideration, and thus present a similar or even lower prediction accuracy than the analysis using peaks. In practice, peak results are composed of informative but incomplete data, while both chemical information and noise are included in the full spectra. Consequently, the use of variable selection methods is required to provide variable sets with high data quality.

Both LDA and PCA-LDA models using either spectral data or peak values present a relatively low accuracy in distinguishing bitumen type and ageing state. To improve the prediction performance, the MW and SA variable selection methods were applied and the prediction results are provided in Tables 2 and 3. Using the MW and SA methods increase the prediction accuracy of LDA and PCA-LDA. The highest accuracy of MW and SA is similar for the prediction of bitumen type and ageing state. The prediction accuracy for bitumen type is 0.75, 0.82, 0.93, and 0.95, and for the classification of ageing state

Table 1. Prediction accuracy of LDA and PCA-LDA models considering peak data and full spectral data.

	Source		Type		Ageing state	
Method	Spectra	Peak	Spectra	Peak	Spectra	Peak
LDA	0.91 (0.09)	1.00 (0.00)	0.75 (0.14)	0.82 (0.08)	0.60 (0.27)	0.65 (0.11)
PCA-LDA	1.00 (0.00)	1.00 (0.00)	0.82 (0.05)	0.83 (0.10)	0.58 (0.24)	0.66 (0.23)

Note: Values in brackets denote the standard deviations of the prediction accuracies for five loops in the 5-fold cross-validation method.

Table 2. Prediction accuracy values of LDA and PCA-LDA models based on MW variable selection method.

	Type			Ageing state		
Window size (cm^{-1})	LDA	PCA-LDA	Band range (cm^{-1})	LDA	PCA-LDA	Band range (cm^{-1})
50	0.86	0.87	1425–1475	0.66	0.71	1650–1700
100	0.91	0.89	2875–2975	0.69	0.71	1225–1325
150	0.92	0.92	2825–2975	0.72	0.74	1600–1750
200	0.93	0.95	2800–3000	0.72	0.75	1600–1800
250	0.90	0.92	2800–3050	0.76	0.76	900–1150
300	0.90	0.90	2650–2950	0.75	0.80	1050–1350
350	0.89	0.91	2650–3000	0.85	0.80	1000–1350
400	0.89	0.91	975–1375	0.80	0.84	1000–1400
450	0.91	0.91	1000–1450	0.78	0.88	900–1350
500	0.85	0.91	950–1450	0.74	0.84	900–1400
550	0.81	0.92	825–1375	0.67	0.86	750–1300
600	0.86	0.93	825–1425	0.62	0.85	700–1300
650	0.89	0.92	850–1500	0.71	0.83	750–1400
700	0.88	0.93	850–1550	0.72	0.83	700–1400
750	0.88	0.93	650–1400	0.75	0.83	825–1575
800	0.89	0.92	600–1400	0.77	0.83	825–1625

Note: The band range is the interval where the highest accuracy of PCA-LDA is obtained.

Table 3. Prediction accuracy values of LDA and PCA-LDA models based on SA variable selection method.

	Type		Ageing state			Type		Ageing state	
Variable number	LDA	PCA-LDA	LDA	PCA-LDA	Variable number	LDA	PCA-LDA	LDA	PCA-LDA
10	0.85	0.83	0.74	0.79	100	0.89	0.9	0.70	0.83
20	0.91	0.85	0.80	0.77	110	0.8	0.93	0.64	0.81
30	0.92	0.88	0.74	0.81	120	0.83	0.89	0.53	0.79
40	0.94	0.86	0.86	0.83	130	0.84	0.92	0.66	0.82
50	0.96	0.90	0.8	0.87	140	0.91	0.91	0.70	0.78
60	0.93	0.96	0.78	0.82	150	0.88	0.93	0.66	0.75
70	0.93	0.94	0.79	0.81	160	0.87	0.91	0.64	0.82
80	0.93	0.89	0.71	0.83	170	0.92	0.91	0.70	0.74
90	0.88	0.93	0.80	0.80	180	0.86	0.93	0.68	0.75

is 0.60, 0.58, 0.85, and 0.88, respectively for the LDA, PCA-LDA, MW-LDA, and MW-PCA-LDA methods. This indicates that the PCA-LDA model has practically better performance than LDA, especially when coupled with variable selection methods.

For the MW-aided discriminant analysis, the prediction results depend on the selection of window size, as shown in Table 2. With increasing window size from 50 to 800 cm^{-1}, the accuracy of both LDA and PCA-LDA models initially increases and then generally decreases. In datasets with window size smaller than ca. 450 cm^{-1}, the selected variables are sufficient to distinguish all the bitumen samples. Additional variables in a larger band interval provide limited chemical information and may contain more noisy and irrelevant variables. As a result, a decrease in the prediction accuracy is achieved. The same trend also holds for the SA variable selection method.

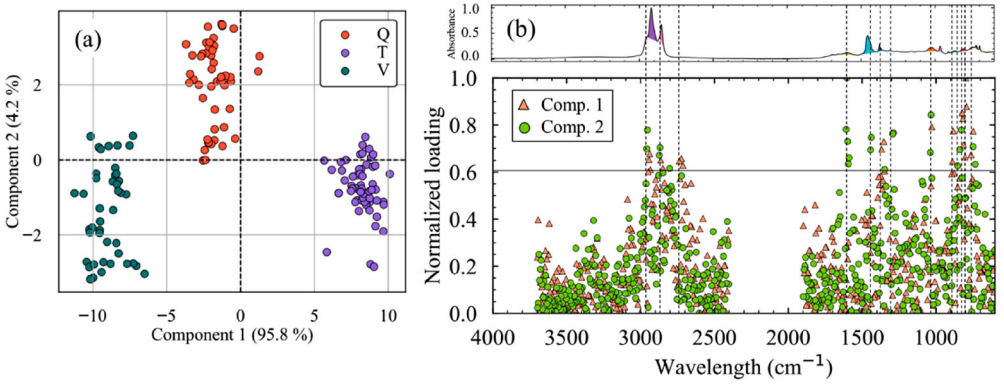

Figure 6. Classification of bitumen sources using PCA-LDA model: (a) score plot and (b) normalised loading plot of full spectra for all 40 samples.

3.3. Classification of bitumen source and type

Figure 6 shows the score and loading plots of bitumen source. Three sources are well distinguished in the score plots. Principal component 1 (PC1) is able to differentiate among the three crude oil sources. The differences in source Q and the other two crude oil sources can be explained by principal component 2 (PC2). Loadings plots are used to determine the specific band regions accounting for the variance in PC1 and PC2. According to the loading plots of PC1 and PC2, the aliphatic C–H stretching and bending in CH_2 and CH_3, the aromatic C = C stretching and C–H bending, and the sulfoxide functional group are the critical peaks in determining bitumen sources. Particularly, the C–H bending (at 700–900 cm^{-1}) and the sulfoxide functional group (peak at 1030 cm^{-1}) differentiate the source Q from other crude oil sources, as shown in the PC2 loading plot. The PC1 and PC2 loading plots show that the samples from source Q have similar C = C content (1600 cm^{-1}) with the samples from the V and T source, while its C–H structure is distinct. Three peaks denoting the aromatic C–H out-of-plane bending at wavenumbers of 877, 810, and 754 cm^{-1} are ascribed to the C–H in isolated adjacent hydrogen aromatic rings, two isolated adjacent hydrogen aromatic rings, and four isolated adjacent hydrogen aromatic rings, respectively (Asemani & Rabbani, 2020). These peaks indicate that the number of adjacent hydrogens and their positions in aromatic rings are different for the Q samples (Castro & Vazquez, 2009). Overall, discriminant analysis shows that the aliphatic and the aromatic content and structure are of key importance for distinguishing different bitumen sources. However, in Figure 3, the relevant band ranges show limited differences. In fact, the differences in bitumen sources may not only depend on the intensities of these peaks but also on their positions, shapes, and the intensity ratio between these peaks. Therefore, integrated analysis of all peak regions are required, which can be achieved using discriminant analysis and variable selection methods.

Figure 7 shows the score plots for bitumen type classification. It can be observed that the three penetration grades from source T are closer to each other compared to the two penetration grades from Q. This indicates a higher stability and consistency of source T for different penetration grades.

To identify the critical band areas with regard to the identification of bitumen type, MW screening of the whole band range with a size of 50 cm^{-1} was performed considering peak ranges that are close to or slightly larger than 50 cm^{-1} (note that MW screening is different from the MW variable selection method; screening simply divides the whole spectrum into intervals with the same size, and all intervals are used for discriminant analysis). A loading matrix of optimised band variables using the SA method was also evaluated. As shown in Figure 8, most band areas depicted in Figure 1 show a relatively good accuracy in differentiating bitumen type in the case of MW. Among them, the aliphatic C–H stretching in CH_2 and CH_3 at 3000–2800 cm^{-1}, the aliphatic C–H bending at 1485–1350 cm^{-1}, the aromatic C–H bending at 900–710 cm^{-1}, the aromatic C = C stretching, and sulfoxide stretching

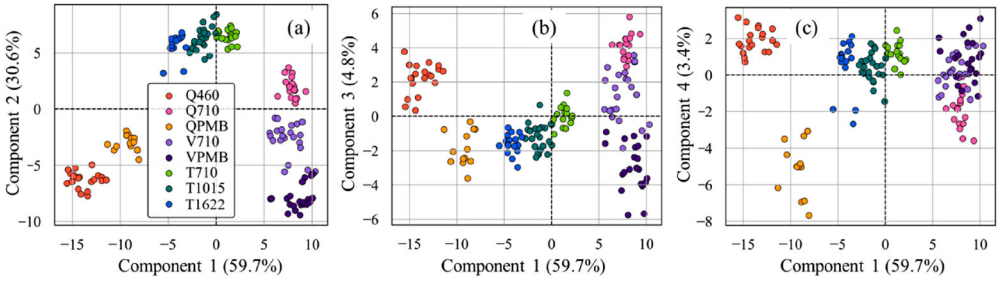

Figure 7. Score plots for bitumen type classification using PCA-LDA model using the full spectra of all (40) samples: (a) PC1 vs. PC2, (b) PC1 vs. PC3, (c) PC1 vs. PC4. The spectra variables were obtained from the dataset with the highest prediction accuracy in the moving-window search results as shown in Table 2.

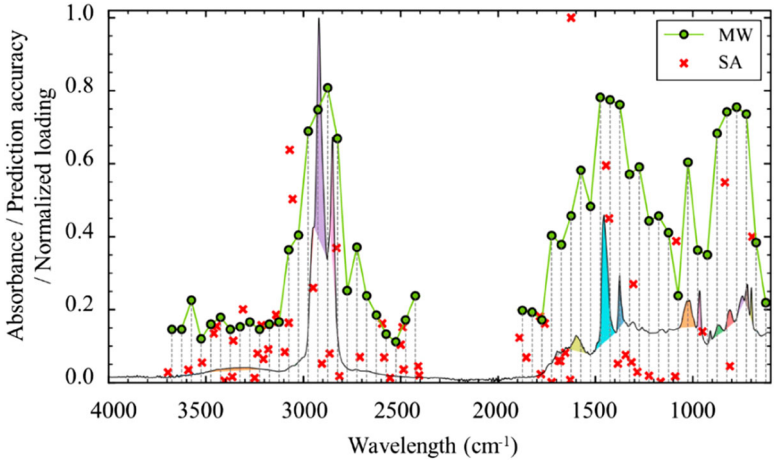

Figure 8. Classification of bitumen type using PCA-LDA model coupled with MW and SA variable selection methods using the full spectra of all (40) samples. For MW, the whole spectrum was divided into 52 intervals with a size of 50 cm^{-1}. The prediction accuracy of every band interval was then calculated. For SA, the normalised loading of the 60 variables selected based on highest prediction accuracy (Table 3) is depicted.

are the peaks with the highest prediction accuracy. Accuracy values up to 0.8 show that the chemical components represented by these band ranges exhibit important differences in all bitumen samples. Expect for the peaks shown in Figure 1, it is noted that band area at 1350–1100 cm^{-1} provides a prediction accuracy of 0.5–0.6. This area is related to heteroatom-atom based functional groups including alcohols, esters, ethers, sulfones, sulfate esters, and amides (Asemani & Rabbani, 2020).

The SA method presents similar peak positions as revealed by the MW method (Figure 8). At band areas of 1485–1350 cm^{-1} and 900–710 cm^{-1}, not all characteristic peaks are selected. Instead, only one to two representative peaks are identified. This indicates that adjacent peaks at these band areas are highly correlated to each other for the same bitumen type and only one or two peaks in this range are capable of describing the bitumen type. The similar prediction accuracies (using the MW window) at wavelengths of 1475, 1425, and 1375 cm^{-1}, and at wavelengths of 875, 825, 775, and 725 cm^{-1} also indicate their similar functionalities for the classification of bitumen type.

3.4. Classification of bitumen ageing state

The differentiation of ageing state is depicted in Figure 9. According to the score results, fresh bitumen and oven-aged bitumen are more difficult to separate compared to other ageing states. This indicates the smaller chemical differences between fresh and oven-aged bitumen compared to other ageing

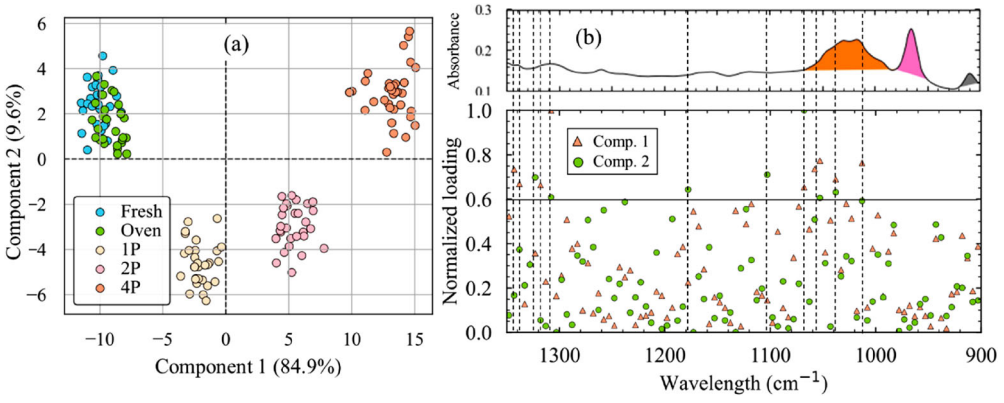

Figure 9. Classification of ageing states: (a) score plot of PCA-LDA model and (b) loading plot of PCA-LDA model. The variables used here are based on the MW results with the highest prediction accuracy, namely the band range from 1350 to 900 cm^{-1} (Table 2).

states. The loading plot of PC1 shows that the bands ranging from 1350 to 1300 cm^{-1} and from 1100 to 1000 cm^{-1} significantly contribute to the chemical changes during ageing process.

Figure 10 describes the prediction accuracy of WM-based PCA-LDA modelling for all band intervals with a length of 50 cm^{-1} and the loading plot obtained from SA-based PCA-LDA modelling using full spectra. Both MW and SA show that the main band ranges related to chemical changes due to ageing are at wavenumbers of ca.1800–900 cm^{-1}. This wavenumber region is related to carbon-related functional groups including esters, ketones, aldehydes, and carboxylic acids (Asemani & Rabbani, 2020), sulfur-containing functional groups such as sulfoxides, sulfones and sulfate ester (Mirwald et al., 2020a), and nitrogen-based amides. These functional groups are involved in chemical reactions during the bitumen ageing process. Among these functional groups, carbonyls and sulfoxides are widely used for evaluating bitumen ageing. The remainder carbon-related, sulfur-containing and nitrogen-based amides functional groups are less investigated because of difficulties associated with peak overlapping and low intensity. Figure 4 demonstrates that the peaks in the range of 1800–900 cm^{-1} change with ageing, but changes are not sufficiently large to be precisely quantified by calculating the intensities or the tangential areas of these peaks.

For the ageing of SBS-modified bitumen, both SA and MW detects the peak at 966 cm^{-1} describing the $=$C–H wagging in trans-alkenes, while the peak at 700 cm^{-1} is less related to ageing. This finding indicates that during the ageing of SBS-modified bitumens is mainly associated to the degradation of polybutadiene due to chain scission (Nivitha et al., 2016).

4. Conclusions

This paper investigates the classification of bitumen source, bitumen type, and ageing state using principal component analysis (PCA) and linear discriminant analysis (LDA) models. To increase the efficiency and accuracy of the coupled PCA-LDA analysis, the chemometric methods were combined with the moving window (MW) and the simulated annealing (SA) variable selection methods. The analysis revealed the essential wavenumber band areas that indicate chemical changes responsible for the identification of bitumen type and ageing state.

The classification analysis results demonstrate that PCA-LDA shows better performance than LDA when variable selection methods are applied. The prediction accuracy values of bitumen source, type, and ageing state are 1.0, 0.96, and 0.88, indicating a good differentiation of bitumen samples using the LDA and PCA-LDA when coupled with variable selection methods.

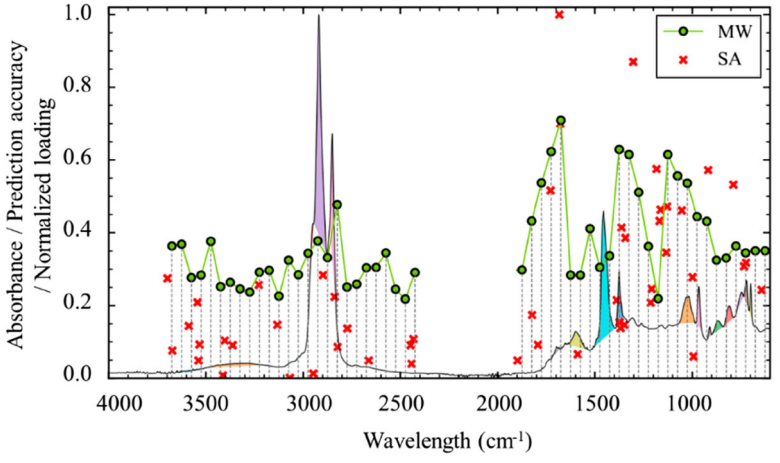

Figure 10. Classification of ageing states using PCA-LDA model coupled with MW and SA variable selection methods for the full spectra of all (40) samples. For MW, the whole spectrum was divided into 52 intervals with a size of 50 cm^{-1}. The prediction accuracy of each band interval was computed. For SA, the normalised loading of the 50 variables selected based on highest prediction accuracy (Table 3) is depicted.

The main chemical components associated with the classification of bitumen sources and types are the aliphatic and aromatic bond vibrations at wavenumbers of ca. 3000–2880 cm^{-1}, 1350–1500 cm^{-1}, and 750–900 cm^{-1}, as well as the sulfoxide group. Bands areas at wavenumbers of ca. 1800–900 cm^{-1}, which reveal the chemical changes of heteroatom-based functional groups, are found to be critical to the classification of ageing state.

This work shows that chemometric analysis combined with variable selection methods is able to identify the main functional groups related to the chemical differences of various bitumen types and ageing states. These chemical information provides new insights into the study of the chemical composition and ageing mechanisms of bituminous binders.

Acknowledgements

LM acknowledges support from the China Scholarship Council (CSC). AV acknowledges NWO-AES (Dutch Research Council-Applied and Engineering Sciences) for a Talent Programme VENI grant for the project 'A multiscale approach towards future road infrastructure: How to design sustainable paving materials?'.

Disclosure statement

No potential conflict of interest was reported by the author(s).

Funding

LM acknowledges support from the China Scholarship Council (CSC). AV acknowledges NWO-AES (Dutch Research Council-Applied and Engineering Sciences) for a Talent Programme VENI grant for the project 'A multiscale approach towards future road infrastructure: How to design sustainable paving materials?'.

ORCID

Aikaterini Varveri http://orcid.org/0000-0002-8830-9437
Ruxin Jing http://orcid.org/0000-0001-6975-807X

References

Asemani, M., & Rabbani, A. R. (2020). Detailed FTIR spectroscopy characterization of crude oil extracted asphaltenes: Curve resolve of overlapping bands. *Journal of Petroleum Science and Engineering*, *185*, 106618. https://doi.org/10.1016/j.petrol.2019.106618

Aske, N., Kallevik, H., & Sjoblom, J. (2001). Determination of saturate, aromatic, resin, and asphaltenic (SARA) components in crude oils by means of Infrared and Near-Infrared spectroscopy. *Energy & Fuels*, *15*(5), 1304–1312. https://doi.org/10.1021/ef010088h

Buenrostro-Gonzalez, E., Andersen, S. I., Garcia-Martinez, J. A., & Lira-Galeana, C. (2002). Solubility/molecular structure relationships of asphaltenes in polar and nonpolar media. *Energy & Fuels*, *16*(3), 732–741. https://doi.org/10.1021/ef0102317

Castro, L. V., & Vazquez, F. (2009). Fractionation and characterization of Mexican crude oils. *Energy & Fuels*, *23*(3), 1603–1609. https://doi.org/10.1021/ef8008508

Dehouche, N., Kaci, M., & Mokhtar, K. A. (2012). Influence of thermo-oxidative aging on chemical composition and physical properties of polymer modified bitumens. *Construction and Building Materials*, *26*(1), 350–356. https://doi.org/10.1016/j.conbuildmat.2011.06.033

Feng, Z.-g., Bian, H.-j., Li, X.-j., & Yu, J.-y. (2015). FTIR analysis of UV aging on bitumen and its fractions. *Materials and Structures*, *49*(4), 1381–1389. https://doi.org/10.1617/s11527-015-0583-9

Gabrienko, A. A., Morozov, E. V., Subramani, V., Martyanov, O. N., & Kazarian, S. G. (2015). Chemical visualization of asphaltenes aggregation processes studied in situ with ATR-FTIR spectroscopic imaging and NMR imaging. *The Journal of Physical Chemistry C*, *119*(5), 2646–2660. https://doi.org/10.1021/jp511891f

Herrington, P. R. (2012). Diffusion and reaction of oxygen in bitumen films. *Fuel*, *94*(1), 86–92. https://doi.org/10.1016/j.fuel.2011.12.021

Hofko, B., Alavi, M. Z., Grothe, H., Jones, D., & Harvey, J. (2017). Repeatability and sensitivity of FTIR ATR spectral analysis methods for bituminous binders. *Materials and Structures*, *50*(3):187. https://doi.org/10.1617/s11527-017-1059-x

Khanmohammadi, M., Garmarudi, A. B., Garmarudi, A. B., & Guardia, M. l. l. (2012). Characterization of petroleum-based products by infrared spectroscopy and chemometrics. *TrAC Trends in Analytical Chemistry*, *35*, 135–149. https://doi.org/10.1016/j.trac.2011.12.006

Kirkpatrick, S., Gelatt, C. D., & Vecchi, J. M. P. (1983). Optimization by simulated annealing. *Science*, *220*(4598), 671–680. https://doi.org/10.1126/science.220.4598.671

Kumar, Y., Singh, S. K., Oberoi, D., Kumar, P., Mohanty, P., & Ravindranath, S. S. (2020). Effect of molecular structure and concentration of styrene-butadiene polymer on upper service temperature rheological properties of modified binders. *Construction and Building Materials*, *249*, 118790. https://doi.org/10.1016/j.conbuildmat.2020.118790

Li, Z., Zhuo, R., Zhao, Y., Cao, Q., & Qin, W. (2019). Discriminating wavenumbers selection of ATR-FTIR spectra for identifying graded asphalt. *Construction and Building Materials*, *214*, 565–573. https://doi.org/10.1016/j.conbuildmat.2019.04.068

López-Montero, T., & Miró, R. (2016). Differences in cracking resistance of asphalt mixtures due to ageing and moisture damage. *Construction and Building Materials*, *112*, 299–306. https://doi.org/10.1016/j.conbuildmat.2016.02.199

Lukas, E., Josef, F., Bernhard, H., Florian, H., Markus, H., Ronald, B., & Hinrich, G. (2015). Towards a microstructural model of bitumen ageing behaviour. *International Journal of Pavement Engineering*, *16*(10), 939–949. https://doi.org/10.1080/10298436.2014.993192

Meléndez, L. V., Lache, A., Orrego-Ruiz, J. A., Pachón, Z., & Mejía-Ospino, E. (2012). Prediction of the SARA analysis of Colombian crude oils using ATR–FTIR spectroscopy and chemometric methods. *Journal of Petroleum Science and Engineering*, *90–91*, 56–60. https://doi.org/10.1016/j.petrol.2012.04.016

Mirwald, J., Werkovits, S., Camargo, I., Maschauer, D., Hofko, B., & Grothe, H. (2020a). Investigating bitumen long-term-ageing in the laboratory by spectroscopic analysis of the SARA fractions. *Construction and Building Materials*, *258*, 119577. https://doi.org/10.1016/j.conbuildmat.2020.119577

Mirwald, J., Werkovits, S., Camargo, I., Maschauer, D., Hofko, B., & Grothe, H. (2020b). Understanding bitumen ageing by investigation of its polarity fractions. *Construction and Building Materials*, *250*, 118809. https://doi.org/10.1016/j.conbuildmat.2020.118809

Mohammadi, M., Khorrami, M. K., Vatani, A., Ghasemzadeh, H., Vatanparast, H., Bahramian, A., & Fallah, A. (2021). Genetic algorithm based support vector machine regression for prediction of SARA analysis in crude oil samples using ATR-FTIR spectroscopy. *Spectrochimica Acta Part A: Molecular and Biomolecular Spectroscopy*, *245*, 118945. https://doi.org/10.1016/j.saa.2020.118945

Nivitha, M. R., Prasad, E., & Krishnan, J. M. (2016). Ageing in modified bitumen using FTIR spectroscopy. *International Journal of Pavement Engineering*, *17*(7), 565–577. https://doi.org/10.1080/10298436.2015.1007230

Petersen, J. C. (2000). Chapter 14 Chemical composition of asphalt as related to asphalt durability. In Teh Fu Yen & George Chilingarian (Eds.), *Developments in petroleum science* (Vol. 40, pp. 363–399). Elsevier.

Petersen, J. C. (2009). A review of the fundamentals of asphalt oxidation chemical, physicochemical, physical property, and durability relationships. *Transport Research Circular Number E-C140*.

Pipintakos, G., Lommaert, C., Varveri, A., & Van den bergh, W. (2022). Do chemistry and rheology follow the same laboratory ageing trends in bitumen? *Materials and Structures*, *55*(5), 146. https://doi.org/10.1617/s11527-022-01986-w

Pipintakos, G., Soenen, H., Ching, H. Y. V., Velde, C. V., Doorslaer, S. V., Lemière, F., Varveri, A., & Van den bergh, W. (2021). Exploring the oxidative mechanisms of bitumen after laboratory short- and long-term ageing. *Construction and Building Materials*, *289*, 123182. https://doi.org/10.1016/j.conbuildmat.2021.123182

Polo-Mendoza, R., Martinez-Arguelles, G., Walubita, L. F., Moreno-Navarro, F., Giustozzi, F., Fuentes, L., & Navarro-Donado, T. (2022). Ultraviolet ageing of bituminous materials: A comprehensive literature review from 2011 to 2022. *Construction and Building Materials*, *350*, 128889. https://doi.org/10.1016/j.conbuildmat.2022.128889

Redelius, P., & Soenen, H. (2015). Relation between bitumen chemistry and performance. *Fuel*, *140*, 34–43. https://doi.org/10.1016/j.fuel.2014.09.044

Ren, R., Han, K., Zhao, P., Shi, J., Zhao, L., Gao, D., Zhang, Z., & Yang, Z. (2019). Identification of asphalt fingerprints based on ATR-FTIR spectroscopy and principal component-linear discriminant analysis. *Construction and Building Materials*, *198*, 662–668. https://doi.org/10.1016/j.conbuildmat.2018.12.009

Sakib, N., & Bhasin, A. (2019). Measuring polarity-based distributions (SARA) of bitumen using simplified chromatographic techniques. *International Journal of Pavement Engineering*, *20*(12), 1371–1384. https://doi.org/10.1080/10298436.2018.1428972

Sakib, N., Hajj, R., Hure, R., Alomari, A., & Bhasin, A. (2020). Examining the relationship between bitumen polar fractions, rheological performance benchmarks, and tensile strength. *Journal of Materials in Civil Engineering*, *32*(6), 04020143. https://doi.org/10.1061/(asce)mt.1943-5533.0003197

Siroma, R. S., Nguyen, M. L., Hornych, P., Lorino, T., & Chailleux, E. (2021). Clustering aged bitumens through multivariate statistical analyses using phase angle master curve. *Road Materials and Pavement Design*, *22*(1), S51–S68. https://doi.org/10.1080/14680629.2021.1907217

Sun, X. T., Yuan, H. F., Song, C. F., Deng, X. X., Lv, G. L., Li, X. Y., & Hu, A. Q. (2020). Rapid and simultaneous determination of physical and chemical properties of asphalt by ATR-FTIR spectroscopy combined with a novel calibration-free method. *Construction and Building Materials*, *230*, 116950. https://doi.org/10.1016/j.conbuildmat.2019.116950

Tauste, R., Moreno-Navarro, F., Sol-Sánchez, M., & Rubio-Gámez, M. C. (2018). Understanding the bitumen ageing phenomenon: A review. *Construction and Building Materials*, *192*, 593–609. https://doi.org/10.1016/j.conbuildmat.2018.10.169

Weigel, S., & Stephan, D. (2017). The prediction of bitumen properties based on FTIR and multivariate analysis methods. *Fuel*, *208*, 655–661. https://doi.org/10.1016/j.fuel.2017.07.048

Weigel, S., & Stephan, D. (2018). Differentiation of bitumen according to the refinery and ageing state based on FTIR spectroscopy and multivariate analysis methods. *Materials and Structures*, *51*(5), 130. https://doi.org/10.1617/s11527-018-1252-6

Wilt, B. K., & Welch, W. T. (1998). Determination of asphaltenes in petroleum crude oils by Fourier Transform Infrared Spectroscopy. *Energy & Fuels*, *12*(5), 1008–1012. https://doi.org/10.1021/ef980078p

Xiaobo, Z., Jiewen, Z., Povey, M. J., Holmes, M., & Hanpin, M. (2010). Variables selection methods in near-infrared spectroscopy. *Analytica Chimica Acta*, *667*(1–2), 14–32. https://doi.org/10.1016/j.aca.2010.03.048

Zojaji, I., Esfandiarian, A., & Taheri-Shakib, J. (2021). Toward molecular characterization of asphaltene from different origins under different conditions by means of FT-IR spectroscopy. *Advances in Colloid and Interface Science*, *289*, 102314. https://doi.org/10.1016/j.cis.2020.102314